Geophysical Research Letters

RESEARCH LETTER
10.1029/2024GL108406

Decadal Variability of Ice-Shelf Melting in the Amundsen Sea Driven by Sea-Ice Freshwater Fluxes

Michael Haigh[1] and **Paul R. Holland**[1]

[1]British Antarctic Survey, Cambridge, UK

Key Points:

- In the Amundsen Sea decadal variability of an undercurrent flowing along the shelf break drives decadal variability in ice-shelf basal melt
- Sea-ice freshwater fluxes and positive feedbacks from ice-shelf basal melt drive the undercurrent variability
- Tropical Pacific teleconnections induce atmospheric anomalies over the Amundsen Sea which drive the sea-ice freshwater flux variability

Supporting Information:

Supporting Information may be found in the online version of this article.

Correspondence to:

M. Haigh,
michai@bas.ac.uk

Citation:

Haigh, M., & Holland, P. R. (2024). Decadal variability of ice-shelf melting in the Amundsen Sea driven by sea-ice freshwater fluxes. *Geophysical Research Letters*, *51*, e2024GL108406. https://doi.org/10.1029/2024GL108406

Received 18 JAN 2024
Accepted 15 APR 2024

Author Contributions:

Conceptualization: Michael Haigh, Paul R. Holland
Data curation: Paul R. Holland
Formal analysis: Michael Haigh, Paul R. Holland
Funding acquisition: Paul R. Holland
Investigation: Michael Haigh
Methodology: Michael Haigh, Paul R. Holland
Project administration: Paul R. Holland
Resources: Paul R. Holland
Software: Michael Haigh, Paul R. Holland
Supervision: Paul R. Holland
Validation: Michael Haigh
Visualization: Michael Haigh
Writing – original draft: Michael Haigh
Writing – review & editing: Paul R. Holland

Abstract The ice streams flowing into the Amundsen Sea, West Antarctica, are losing mass due to changes in oceanic basal melting of their floating ice shelves. Rapid ice-shelf melting is sustained by the delivery of warm Circumpolar Deep Water to the ice-shelf cavities, which is first supplied to the continental shelf by an undercurrent that flows eastward along the shelf break. Temporal variability of this undercurrent controls ice-shelf basal melt variability. Recent work shows that on decadal timescales the undercurrent variability opposes surface wind variability. Using a regional model, we show that undercurrent variability is induced by sea-ice freshwater fluxes, particularly those north of the shelf break, which affect the cross-shelf break density gradient. This sea-ice variability is linked to tropical Pacific variability impacting atmospheric conditions over the Amundsen Sea. Ice-shelf melting also feeds back onto the undercurrent by affecting the on-shelf density, thereby influencing shelf-break density gradient anomalies.

Plain Language Summary The glaciers that flow toward the Amundsen Sea, West Antarctica, are losing ice faster than most others about the continent. Once these glaciers reach the coast, they extend out onto the ocean surface, forming ice shelves. The rapid loss of ice is caused by changes in melting by relatively warm ocean waters beneath the floating ice shelves. In the Amundsen Sea, a deep ocean current is responsible for delivering warm water from the deep ocean to the ice shelves. We present model results that show that this deep current varies on decadal timescales as a consequence of systematic sea-ice melt and formation patterns. A faster current drives more rapid ice shelf melting which, via a feedback process, further accelerates the current. Climate variability originating in the tropical Pacific Ocean is responsible for the variability in the sea-ice, and is therefore also responsible for the effects on melting of the ice shelves.

1. Introduction

Melting of the West Antarctic Ice Sheet provides Antarctica's biggest contribution to global sea-level rise (Shepherd et al., 2018), with the ice streams draining into the Amundsen Sea of particular concern (Joughin et al., 2014; Rignot et al., 2014). Rapid ice loss in this region is due to the access of warm Circumpolar Deep Water (CDW) to the undersides of the ice shelves, the floating extensions of the grounded ice streams (Heywood et al., 2016; Jacobs et al., 1996). Ocean modeling studies suggest that this basal melting increased over the twentieth century due to anthropogenic forcing (Naughten et al., 2022), and will continue to increase during the 21st century (Jourdain et al., 2022; Naughten et al., 2023). Superimposed on any such long-term trends are the impacts of strong natural decadal climate variability (Dutrieux et al., 2014; Jenkins et al., 2018), on which we focus in this study.

Access of CDW to the Amundsen Sea ice shelves is controlled by an undercurrent that flows eastward along the continental shelf break. As observed (Assmann et al., 2013; Walker et al., 2007, 2013) and modeled (Kimura et al., 2017; Thoma et al., 2008; Webber et al., 2019), the undercurrent is diverted onto the continental shelf when it reaches bathymetric troughs that intersect the shelf break. Through this process the undercurrent transports warm CDW onto the continental shelf, which then flows across the shelf and beneath the ice shelves. Changes in the undercurrent control the variability of ice-shelf melting (Dotto et al., 2019, 2020; Jenkins et al., 2016) and are implicated in historical and future changes in melting (Naughten et al., 2022, 2023). Understanding drivers of undercurrent variability is essential for understanding future melt of the vulnerable ice streams in the Amundsen Sea region.

The undercurrent exists due to the Antarctic Slope Front (ASF), which separates CDW north of the shelf break from the lighter, cooler and fresher waters to the south (Jacobs, 1991; Stewart et al., 2019). This creates a south-to-north pressure gradient which causes the flow to be more eastward with depth. Variability in the ASF, or wider

ocean density variability, will drive baroclinic (depth-dependent) variability in the undercurrent. The density structure across the shelf break can be affected by many processes, including wind-driven downwelling/upwelling (Spence et al., 2014), surface buoyancy fluxes (Caillet et al., 2023), and ice-shelf basal melting (Moorman et al., 2020; Si et al., 2023).

Winds drive barotropic (depth-independent) variability in the undercurrent by influencing gradients in sea-surface height (Assmann et al., 2013). This is thought to be the dominant mechanism on short (synoptic to interannual) timescales (Wåhlin et al., 2013). However, the Amundsen Sea is impacted by slower natural and anthropogenic climate changes that vary on interannual, interdecadal, and centennial timescales (Holland et al., 2022; Steig et al., 2012). Recently, Silvano et al. (2022) presented model output showing that undercurrent variability actually opposes surface wind variability on decadal timescales, such that eastward (westward) shelf-break wind anomalies coincide with a weaker (stronger) eastward undercurrent, while the surface flow variability simply follows the winds. Silvano et al. (2022) suggested that this may be due to wind-driven upwelling/downwelling anomalies on the continental shelf driving slow baroclinic variability that outweighs the faster barotropic effects of the shelf-break winds. In this study we examine the same regional model and demonstrate that this decadal baroclinic variability is primarily driven by sea-ice and ice-shelf freshwater fluxes, consistent with the results of Caillet et al. (2023).

2. Methods

2.1. Amundsen Sea Regional Model

Following Silvano et al. (2022), we use the Massachusetts Institute of Technology general circulation model (MITgcm) including ocean, sea-ice and ice-shelf components, with the same configuration as Naughten et al. (2022) with one minor difference in the application of iceberg meltwater. The model domain spans the longitudes 140° to 80°W and latitudes 75.5° to 62°S, and is discretized onto a 0.1° grid. The vertical direction is discretized by 50 levels with the thinnest (10 m) levels near the surface and the thickest (200 m) levels near the ocean bottom. The model is forced by six-hourly ERA5 (Hersbach et al., 2020) 10 m winds, surface longwave and shortwave radiation, 2 m air temperature, 2 m specific humidity, precipitation and atmospheric pressure. The model is spun up using the 1979–2002 interval of the external forcing data. After this spinup, the forcing is restarted from 1979 and the model is run until 2019 with monthly mean output. Our analysis is based on model output during 1984–2019. Further model details can be found in Naughten et al. (2022).

2.2. Definition of the Undercurrent

The eastward undercurrent is defined using an approach similar to Silvano et al. (2022). We start by locating the 1,000 m isobath at the shelf break between 125° and 108°W, the undercurrent longitudes of interest. For each longitude along the isobath, the along-slope flow beneath the 1,028 kg m^{-3} isopycnal and above 800 m depth is averaged over a meridional range of three grid points either side of the isobath. The undercurrent speed is then defined as the maximum of these meridionally averaged values at any depth, which typically occurs near 500 m depth. The along-slope surface current and winds are computed at each longitude as an average over the same meridional range. All quantities are then averaged along the undercurrent pathway, with the Dotson-Getz and Pine Island-Thwaites West troughs excluded from the computations. Using alternate undercurrent definitions does not affect our conclusions.

2.3. Statistical Methods

We use a combination of correlations and composites to analyze model output. For correlations we use the Pearson correlation coefficient r and significance p, the latter computed using a two-sided Student's t-test. When computing the significance we account for the effective degrees of freedom, defined as the number of time samples divided by twice the e-folding decorrelation timescale. Doing this is important since we focus on decadal variability, but have model output spanning only a few decades. For the same reason, not all provided correlations are significant at the 95% level. Significance values will be provided with each correlation coefficient.

For composites of a response field against a scalar predictor, the positive (negative) composite is computed by averaging anomalies of the response field over all months for which the predictor is half a standard deviation greater (less) than its mean. We use two predictors: the undercurrent speed timeseries described above, and the

Tripole Index (TPI) of the Interdecadal Pacific Oscillation (IPO). We find the Southern Annular Mode to not be significantly correlated with the undercurrent or any other variables of interest, and this is therefore not considered further.

We use the TPI as a means to quantify the influence of tropical Pacific variability, which dominates variability in the Amundsen Sea (Dutrieux et al., 2014; Steig et al., 2012). Previous studies have separated this variability into two modes: El Niño-Southern Oscillation (ENSO) on shorter timescales and the IPO on longer (>13-year) timescales (Li et al., 2021; Newman et al., 2016). The monthly TPI is designed to quantify the longer IPO variability (Henley et al., 2015), but is also highly correlated to all ENSO indices (Holland et al., 2019). Since the timescale under consideration here is intermediate between ENSO and IPO, we use the monthly TPI index to represent all Pacific variability, without ascribing the variability to either mode. In this study, all timeseries are detrended, deseasoned and have a 5-year running mean applied. The only exception is in Section 3.3, where we consider tropical Pacific impacts on wintertime atmospheric fields over the Amundsen Sea.

3. Results

3.1. The Amundsen Sea Undercurrent

Figure 1a shows the time-mean (1984–2019) flow and potential temperature at 455 m depth. The eastward undercurrent follows the continental slope and is guided southwards onto the shelf by bathymetric troughs at the shelf break. Through this process warm CDW is advected onto the continental shelf, and eventually toward the ice shelves.

Figure 1b shows timeseries of the along-slope undercurrent, surface current, surface winds and the ice-shelf basal melt integrated over all the ice shelves shown in Figure 1a. Getz Ice Shelf west of 125°W is omitted from this computation since this part of its cavity is not supplied with CDW by the undercurrent. As first reported by Silvano et al. (2022), on decadal timescales the undercurrent is anticorrelated with the surface current ($r = -0.62$, $p = 0.09$) and weakly anticorrelated with the winds ($r = -0.26$, $p = 0.48$). The role of the undercurrent in controlling the ice-shelf basal melt is reflected in the strong positive correlation ($r = 0.96$, $p < 0.05$) between these two timeseries.

3.2. Density Anomalies and Freshwater Fluxes

Figure 2a shows the time-mean cross-slope density and along-slope velocity averaged along the undercurrent pathway, with y-coordinate centered on the 1,000 m isobath. The southward deepening of density contours over the shelf break represents the ASF. Although the ASF is typically weaker in the Amundsen Sea compared to other sectors about Antarctica, it is nonetheless strong enough for the time-mean flow to transition from weak westward flow near the surface to strong eastward flow at 300–500 m depth. The time-mean ASF is maintained by westward coastal winds and ice-shelf freshwater input. To illustrate this, the time-mean winds, time-mean ice-shelf freshwater flux (positive values freshen the ocean) as well as the time-mean sea-ice freshwater flux are shown in Figure 2b. Westward coastal winds drive Ekman transport toward the coast, inducing coastal downwelling that pushes isopycnals on the continental shelf downwards, contributing to the cross-shelf break density gradient. Freshwater input by ice-shelf melting reduces the density on the continental shelf, further contributing to the cross-shelf break density gradient.

Figures 2c and 2e show composites using the undercurrent speed as the predictor and the along-slope velocity and cross-slope density as response fields. Eastward (westward) undercurrent anomalies coincide with negative (positive) density anomalies on the continental shelf that span most of the water column, and positive (negative) density anomalies north of the shelf break concentrated in the top 50 m of the water column. Cross-slope pressure gradient anomalies (not shown) very closely resemble undercurrent anomalies, confirming that the undercurrent decadal variability is both geostrophic and caused by these density anomalies.

Winds and freshwater fluxes are both potential drivers of the density and undercurrent variability. Figures 2d and 2f show composites of the wind and freshwater flux responses to the undercurrent speed predictor. The wind composites can be used to test the suggestion of Silvano et al. (2022) that anomalous wind-driven upwelling/downwelling on the continental shelf raises/lowers isopycnals on the shelf, reduces/increases the cross-slope density gradient, and consequently decelerates/accelerates the undercurrent. Coastal wind anomalies (Figures 2d and 2f) tend to be weak and, importantly, are not oriented in the direction required to support this concept.

10.1029/2024GL108406

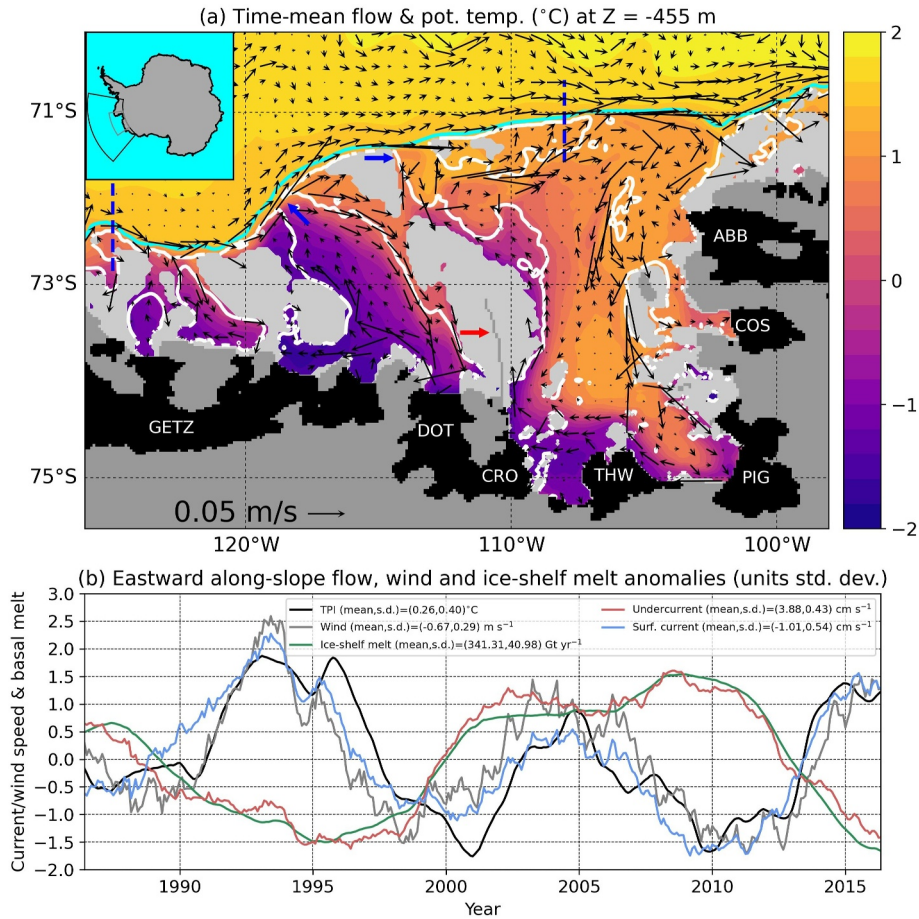

Figure 1. (a) Time-mean flow (arrows, every six grid points) and potential temperature (color, °C) at 455 m depth from model output. The cyan (white) contour represents the 1,000 m (500 m) isobath. Light gray masking represents bathymetry shallower than 455 m, dark gray masking represents land and black masking represents the ice shelves (GETZ = Getz, DOT = Dotson, CRO = Crosson, THW = Thwaites, PIG = Pine Island Glacier, COS = Cosgrove, ABB = Abbot). Blue arrows indicate the Dotson-Getz and Pine Island-Thwaites West troughs. The red arrow indicates Bear Ridge, on which grounded icebergs sit. Inset: map showing model domain (black box) and subregion shown in this figure (gray box). (b) Timeseries of along-slope undercurrent, surface current, winds, area-integrated ice-shelf basal melt and Tripole Index. Timeseries are demeaned and normalized by their standard deviations (see legend).

For example, during eastward undercurrent anomalies, coastal wind anomalies are predominantly eastward which would induce coastal upwelling anomalies, raise isopycnals on the shelf and weaken, rather than strengthen, the shelf-break baroclinicity/undercurrent.

We can test further if on-shelf upwelling/downwelling drives the undercurrent variability by considering the surface stress, which accounts for the combined mechanical forcing by the winds and sea ice (Holland et al., 2019). Composites of the surface stress and surface stress curl anomalies with the undercurrent as predictor (Figure S1 in Supporting Information S1) also suggest that upwelling/downwelling does not drive the undercurrent variability. Coastal surface stress anomalies do not have the necessary orientation and surface stress curl anomalies do not have the necessary sign for either of them to induce the required upwelling/downwelling anomalies. With the evidence suggesting that on-shelf upwelling/downwelling is not responsible for the decadal variability, we move on to consider freshwater fluxes.

The composites in Figures 2d and 2f illustrate how freshwater flux anomalies drive the density and undercurrent variability (Figures 2c and 2e). North of the shelf break, relatively dense (light) surface waters that contribute to eastward (westward) undercurrent anomalies are a result of anomalous sea-ice-driven salinification (freshening). The on-shelf density anomalies, which have sign opposite to those off-shelf, are predominantly due to ice-shelf

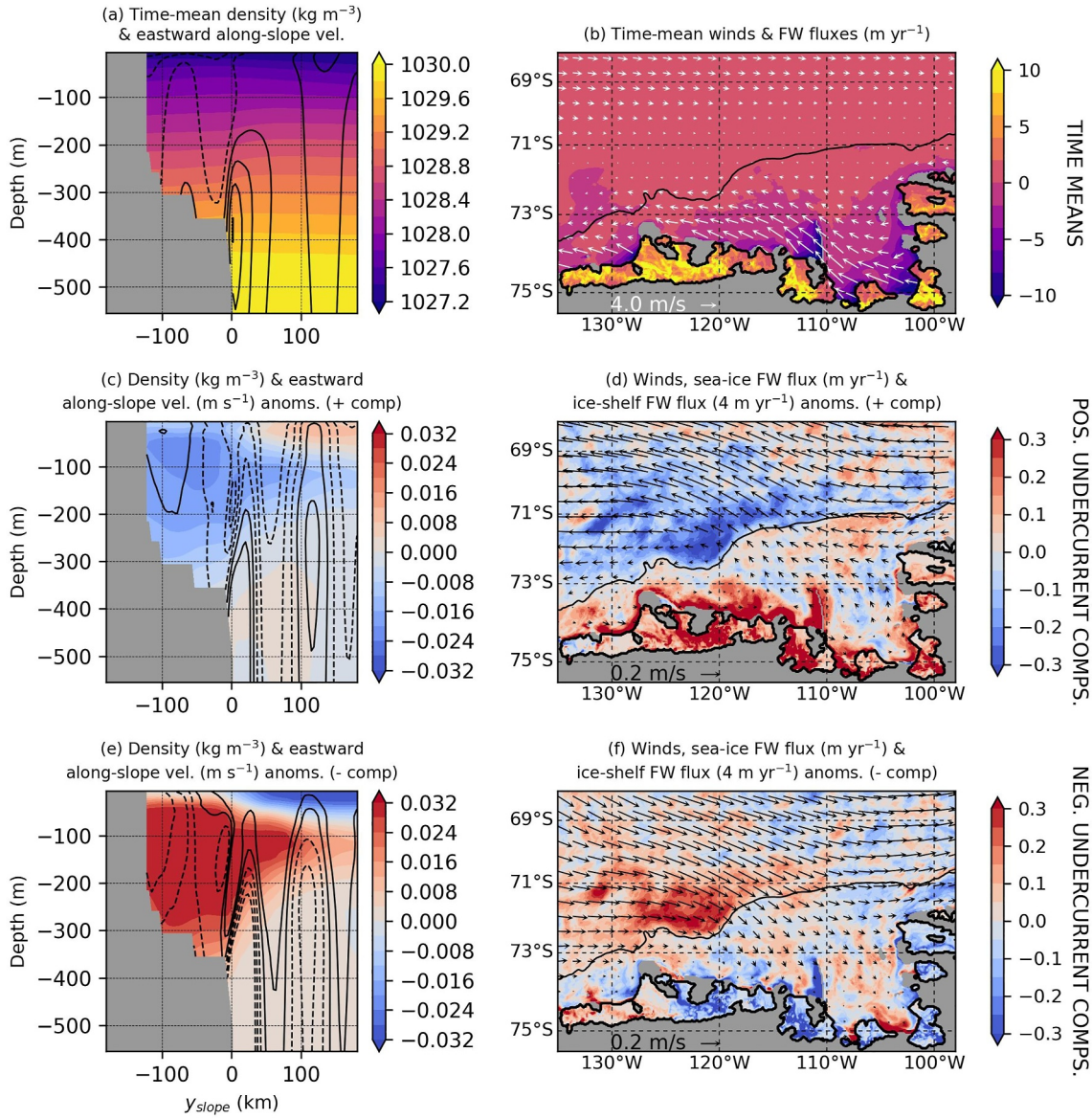

Figure 2. (a) Time-mean density (color, kg m^{-3}) and eastward along-slope velocity (contours, 1 cm s^{-1} contour interval, dashed are zero and negative) averaged along the undercurrent pathway. (b) Time-mean winds (arrows) and sea-ice and ice-shelf freshwater fluxes (color, m yr^{-1}). (c and e) Composites of density and eastward along-slope velocity (1 mm s^{-1} contour interval) for eastward/westward undercurrent anomalies. (d and f) Composites of sea-ice freshwater fluxes (m yr^{-1}), ice-shelf freshwater fluxes (4 m yr^{-1}; units are four times larger than for sea-ice freshwater fluxes) and winds for eastward/westward undercurrent anomalies. In (b, d, f) the thick black contour outlines the ice-shelf drafts and the thin black contour is the 1,000 m shelf-break isobath.

freshwater flux variability. We propose that this ice-shelf melt variability is initially a response to the undercurrent variability driven by sea-ice freshwater fluxes. Then a positive feedback between the undercurrent and ice-shelf melting is initiated, whereby ice-shelf meltwater anomalies impact the on-shelf density and shelf-break density gradient, further enhancing undercurrent anomalies. Over time, the on-shelf density anomalies extrude off of the continental shelf, leading to a reduction in the cross-shelf density gradient and undercurrent anomalies that had previously built up.

During eastward undercurrent anomalies, on-shelf sea-ice freshwater flux anomalies (Figure 2d) have opposite sign to those off-shelf, especially in coastal areas and near Bear Ridge (red arrow, Figure 1a), further contributing to the cross-slope density gradient anomaly. During westward undercurrent anomalies, however, on-shelf sea-ice freshwater flux anomalies (Figure 2f) do not have a distinct spatial pattern.

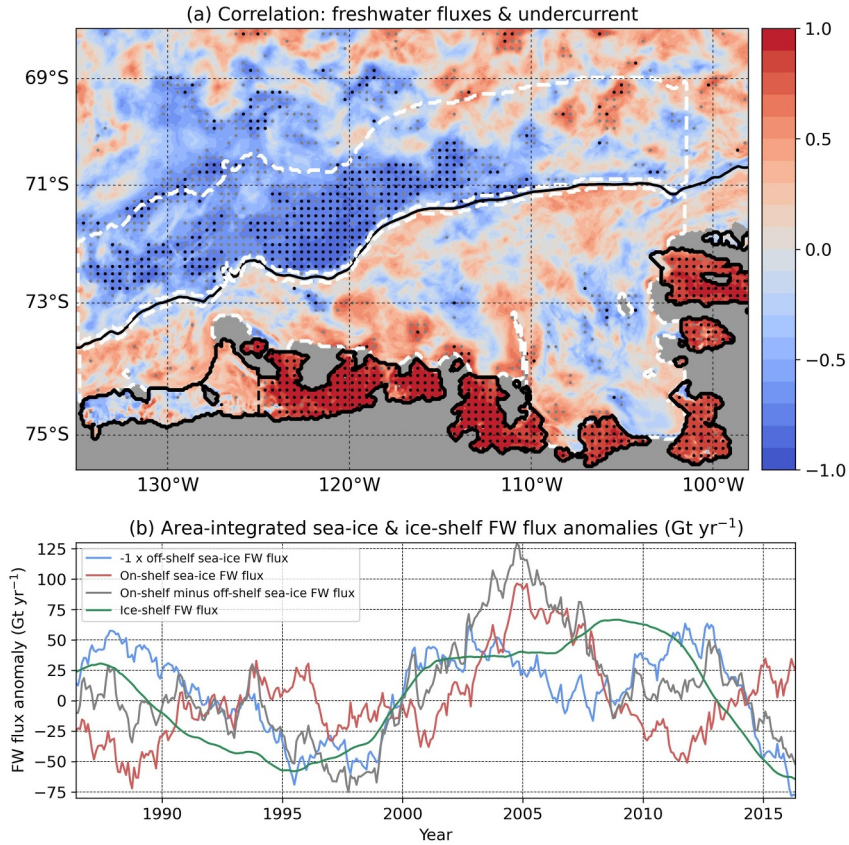

Figure 3. (a) Correlation between the undercurrent speed and the sea-ice and ice-shelf freshwater fluxes. Black (gray) stippling denotes significance $p < 0.05$ ($p < 0.15$). The thick black contour outlines the ice-shelf drafts and the thin black contour is the 1,000 m shelf-break isobath. (b) Timeseries of area-integrated freshwater flux anomalies (Gt yr^{-1}), oriented such that positive values strengthen the undercurrent. Plotted are the on-shelf sea-ice freshwater flux anomaly (red), the negation of the off-shelf sea-ice freshwater flux anomaly (blue), the on-shelf minus off-shelf sea-ice freshwater fluxes (gray) and the ice-shelf freshwater flux anomaly (green). Areas of integration for the sea-ice freshwater fluxes are outlined by the white contours in panel (a). The ice-shelf freshwater flux is integrated over all ice shelves shown in panel (a), excluding the area of the Getz Ice Shelf west of 125°W.

More evidence of the mechanism by which freshwater fluxes drive undercurrent variability is provided by idealized modeling results (Figures S2 and S3 in Supporting Information S1) using the MITgcm configuration of Haigh et al. (2023). In these simulations, decadally varying surface freshwater fluxes are shown to drive a decadally varying undercurrent by impacting the cross-shelf break density gradient. This model does not include ice-shelf freshwater fluxes, suggesting that the surface fluxes alone are sufficient to drive the undercurrent variability.

Figure 3a shows a correlation map with the undercurrent as predictor and sea-ice and ice-shelf freshwater fluxes as response fields, further quantifying the mechanism by which freshwater fluxes drive decadal variability in the undercurrent. The undercurrent negatively correlates ($r \approx 0.8$, $p < 0.05$) with sea-ice freshening anomalies north of the shelf break, but not those downstream of the undercurrent longitudes (east of 108°W). The undercurrent positively correlates (not significant) with sea-ice freshening anomalies over most of the continental shelf. Strong positive correlations ($r \approx 0.9$, $p < 0.05$) between the undercurrent and ice-shelf basal melt reflect the feedback mechanism that exists between the two.

Figure 3b shows timeseries of the sea-ice freshwater flux anomalies, integrated over the on-shelf and off-shelf regions shown in Figure 3a. These regions are selected such that they span the same longitudes and have the same area. Also shown in Figure 3b are timeseries of the difference between the on-shelf and off-shelf freshwater flux anomalies, and the area-integrated ice-shelf freshwater flux anomaly. These timeseries are not sensitive to the precise choice of the areas of integration. The negation of the off-shelf flux anomaly is shown so that, for all timeseries, positive values correspond to an eastward acceleration of the undercurrent.

Area-integrated ice-shelf and sea-ice freshwater flux anomalies have similar magnitude, suggesting that they make similar contributions to the undercurrent decadal variability. The undercurrent negatively correlates with the off-shelf sea-ice freshwater flux ($r = -0.69$, $p < 0.05$), does not notably correlate with the on-shelf sea-ice freshwater flux ($r = 0.20$, $p = 0.62$), but does notably correlate with their difference ($r = 0.71$, $p = 0.08$). These correlations reflect how the integrated off-shelf sea-ice freshwater flux has a distinct decadal variability similar to the undercurrent, whereas the on-shelf sea-ice freshwater flux does not. On-shelf sea-ice freshwater fluxes can nonetheless have large impacts on the on-shelf density and undercurrent, with a large anomaly in 2005 contributing to the ice-shelf basal melt anomaly in 2008. We also highlight that maxima/minima in the undercurrent and ice-shelf basal melt, such as in 2008, can occur before maxima/minima in the off-shelf sea-ice freshwater flux, despite the off-shelf sea-ice freshwater flux being the primary driver of the mechanism described in this study. This is possible because the time at which undercurrent (and hence ice-shelf freshwater flux) anomalies begin to subside is determined by the time at which on-shelf density anomalies extrude off of the continental shelf (Figures 2c and 2e), which can occur before off-shelf sea-ice freshwater flux anomalies are maximized.

3.3. The Role of Tropical Pacific Variability

While decadal variability of ice-shelf basal melt is attributed to the undercurrent, the driver of decadal variability in the sea-ice freshwater fluxes remains to be determined. Here we attribute sea-ice freshwater flux variability to tropical Pacific variability, as quantified by the TPI (Section 2.3). Positive (negative) phases of ENSO and the IPO are typically associated with a filled (deepened) Amundsen Sea Low (ASL) (Clem et al., 2019; Lachlan-Cope & Connolley, 2006). This corresponds to eastward (westward) wind anomalies at the shelf break, which explains the decadal variability of the along-shelf break surface flow and its correlation with the TPI ($r = 0.91$, $p < 0.05$; Figure 1b).

The negative correlation between the undercurrent and the TPI ($r = -0.63$, $p = 0.07$; Figure 1b) is found to be caused by the impacts of Pacific variability on atmospheric conditions over the Amundsen Sea during austral winter (JJA), the season during which tropical teleconnections with the region are strongest (Ding et al., 2011; Li et al., 2021). Figures 4a and 4b show composites of the winter sea-ice freshwater flux anomaly during positive and negative phases of the TPI. Similar to the relationship between freshwater fluxes and undercurrent speed (Figures 2 and 3), there is anomalous sea-ice-driven freshening (salinification) north of the shelf break during positive (negative) composites of the TPI. The spatial distribution of the on-shelf sea-ice freshwater flux anomaly is less distinct, and its sign tends to follow the anomaly north of the shelf break.

Figures 4c and 4d show composites of the ERA5 10 m winds and 2 m air temperature responses to the TPI predictor, and Figures 4e and 4f show composites of the downward longwave radiation and 2 m specific humidity responses. During positive phases of the TPI, the weakened ASL creates northerly wind anomalies over the deep ocean. This transports relatively warm and moist air southwards over the region north of the shelf break, leading to greater downward longwave radiation. Consequently, during positive phases of the TPI, all of the wintertime sea-ice surface heat fluxes (sensible and latent heat fluxes and longwave radiation) are anomalously downwards, leading to a reduction in sea-ice formation and even periods of absolute sea-ice melt north of the shelf break. During negative phases of the TPI the opposite process occurs, causing greater sea-ice formation north of the shelf break.

In either phase of the TPI, anomalies in thermodynamic atmospheric fields on the continental shelf have the opposite sign to anomalies north of the shelf break. However, freshwater flux anomalies on the continental shelf tend to have the same sign as anomalies north of the shelf break. This behavior can be explained by winds near the coast: during negative phases of the TPI, wind anomalies tend to be directed away from the coast, opening coastal polynyas, increasing sea-ice formation and brine rejection. During positive TPI phases, the opposite process occurs, although the coastal wind anomalies are weaker. The contrasting effects of coastal winds and thermodynamic atmospheric anomalies cause the lack of distinct decadal variability in the on-shelf sea-ice freshwater fluxes compared to the off-shelf fluxes (Figure 3b).

4. Discussion and Conclusions

Understanding the variability of the Amundsen Sea eastward undercurrent is important since it modulates basal melting of the ice shelves in the region. Until recently the undercurrent was thought to simply vary with the winds

10.1029/2024GL108406

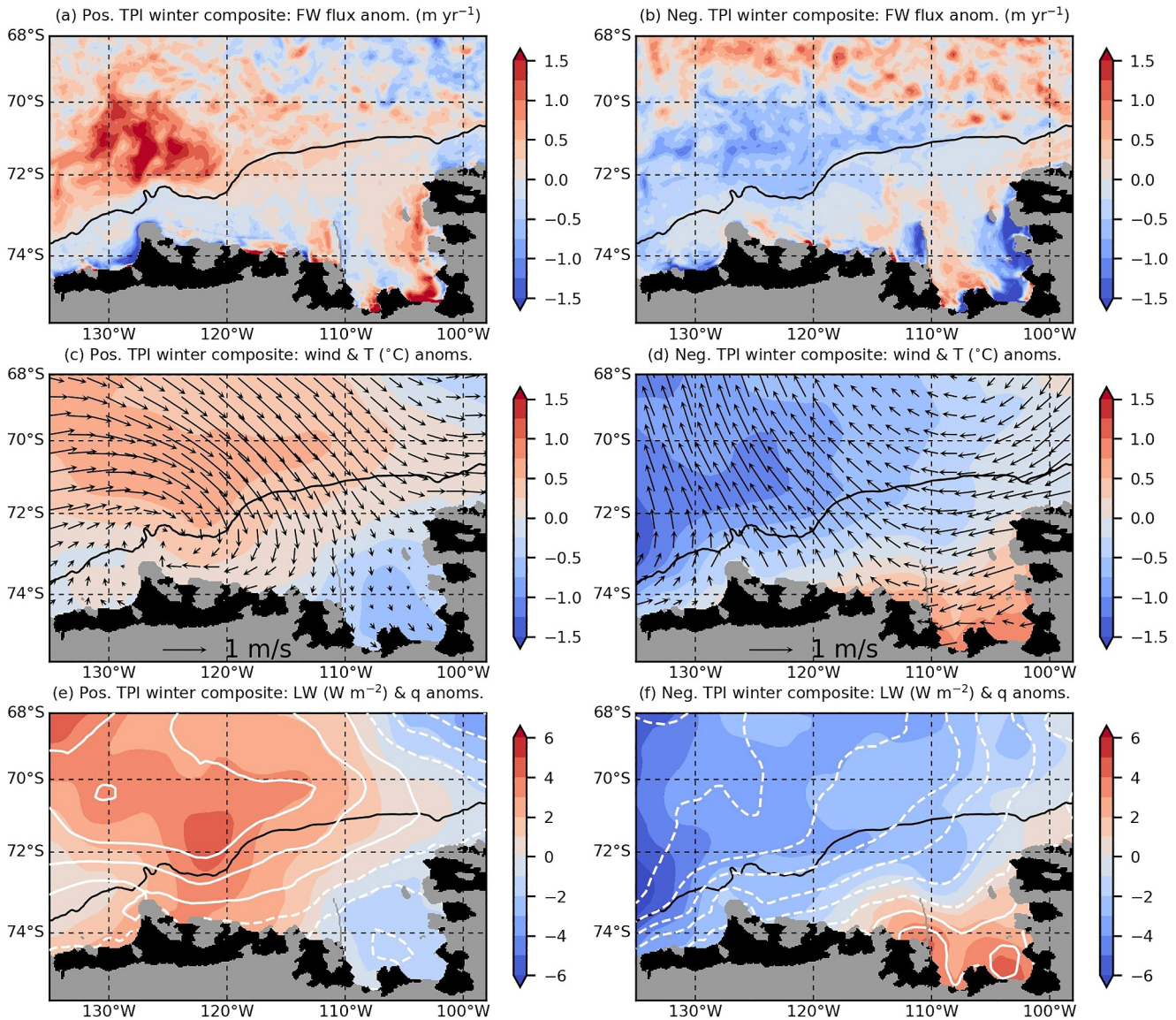

Figure 4. Winter (JJA) composites using the Tripole Index (TPI) as the predictor and freshwater fluxes and atmospheric conditions as the response fields. (a and b) Composites of the winter sea-ice freshwater flux anomaly (m yr^{-1}) during positive/negative TPI. (c and d) Composites of the winter 10 m wind (arrows) and 2 m air temperature, T (color, °C) during positive/negative TPI. (e and f) Composites of the winter downward longwave radiation (color, W m^{-2}) and 2 m specific humidity, q (white contours, 2.5 × 10^{-5} kg kg^{-1} contour interval, dashed are zero and negative) during positive/negative TPI.

over the continental shelf break. However, Silvano et al. (2022) presented model results showing that on decadal timescales the undercurrent variability actually opposes wind variability. In this study we show that this undercurrent decadal variability is driven by a combination of sea-ice and ice-shelf freshwater fluxes, consistent with Caillet et al. (2023).

Composites of regional model output show that on decadal timescales eastward (westward) undercurrent anomalies are due to anomalous sea-ice-driven salinification (freshening) north of the shelf break which enhances (weakens) the cross-slope baroclinicity. Decadal variability in the sea-ice freshwater flux is due to tropical Pacific variability and its impacts on the ASL and local atmospheric conditions during winter (Clem et al., 2019; Lachlan-Cope & Connolley, 2006). Periods of faster (slower) undercurrent lead to enhanced (reduced) ice-shelf basal melt. The ice-shelf basal melt anomalies create on-shelf density anomalies which reinforce the anomalies in the cross-slope pressure gradient and undercurrent.

The conclusions of our study are based on one regional model simulation spanning just two periods of the decadal variability. For this reason presented timeseries have few effective degrees of freedom, meaning some provided correlations are not significant at the 95% level. For example, while the correlation between the undercurrent and off-shelf sea-ice freshwater flux is significant ($r = -0.69$, $p < 0.05$), the correlation between the TPI and the off-shelf fluxes ($r = 0.53$, $p = 0.15$) is not. As such, further modeling efforts are necessary to gain confidence in the link to tropical Pacific variability.

In addition to natural decadal variability, the Amundsen Sea region is impacted by anthropogenic effects, driving trends in the regional winds (Goyal et al., 2021; Holland et al., 2022) which can drive trends in ocean conditions, in particular increasing the on-shelf heat content (Naughten et al., 2022; Spence et al., 2014). Climate projections show that ice-shelf basal melt in the Amundsen Sea is expected to increase over the next century (Jourdain et al., 2022; Naughten et al., 2023). In the simulations of Naughten et al. (2023), this trend is driven by the undercurrent, which in the RCP 8.5 scenario causes the ice shelves to become perpetually bathed in warm CDW. In this high-emissions scenario decadal variability would have little additional influence on ice-shelf basal melt, as is the case in the perturbation experiments of Caillet et al. (2023). In contrast, in lower-emissions scenarios decadal variability would likely remain important. Improving our understanding of both the anthropogenic trends and the natural variability remains a crucial challenge which must be tackled for society to mitigate against and adapt to future sea-level rise.

Data Availability Statement

The data and post-processing codes used in this study are available for download from Haigh and Holland (2024). Data for the Tripole Index (Henley et al., 2015) for the Interdecadal Pacific Oscillation can be found at https://psl.noaa.gov/data/timeseries/IPOTPI/.

Acknowledgments
This research was funded by the NERC project "Drivers of Oceanic Change in the Amundsen Sea," NE/T012803/1.

References

Assmann, K. M., Jenkins, A., Shoosmith, D. R., Walker, D. P., Jacobs, S. S., & Nicholls, K. W. (2013). Variability of circumpolar deep water transport onto the Amundsen Sea continental shelf through a shelf break trough. *Journal of Geophysical Research: Oceans*, *118*(12), 6603–6620. https://doi.org/10.1002/2013jc008871

Caillet, J., Jourdain, N. C., Mathiot, P., Hellmer, H. H., & Mouginot, J. (2023). Drivers and reversibility of abrupt ocean state transitions in the Amundsen Sea, Antarctica. *Journal of Geophysical Research: Oceans*, *128*(1), e2022JC018929. https://doi.org/10.1029/2022JC018929

Clem, K. R., Lintner, B. R., Broccoli, A. J., & Miller, J. R. (2019). Role of the South Pacific convergence zone in West Antarctic decadal climate variability. *Geophysical Research Letters*, *46*(12), 6900–6909. https://doi.org/10.1029/2019gl082108

Ding, Q., Steig, E. J., Battisti, D. S., & Küttel, M. (2011). Winter warming in West Antarctica caused by central tropical Pacific warming. *Nature Geoscience*, *4*(6), 398–403. https://doi.org/10.1038/ngeo1129

Dotto, T. S., Garabato, A. C. N., Bacon, S., Holland, P. R., Kimura, S., Firing, Y. L., et al. (2019). Wind-driven processes controlling oceanic heat delivery to the Amundsen Sea, Antarctica. *Journal of Physical Oceanography*, *49*(11), 2829–2849. https://doi.org/10.1175/jpo-d-19-0064.1

Dotto, T. S., Garabato, A. C. N., Wåhlin, A. K., Bacon, S., Holland, P. R., Kimura, S., et al. (2020). Control of the oceanic heat content of the Getz-Dotson Trough, Antarctica, by the Amundsen Sea Low. *Journal of Geophysical Research: Oceans*, *125*(8), e2020JC016113. https://doi.org/10.1029/2020jc016113

Dutrieux, P., Rydt, J. D., Jenkins, A., Holland, P. R., Ha, H. K., Lee, S. H., et al. (2014). Strong sensitivity of Pine Island ice-shelf melting to climatic variability. *Science*, *343*(6167), 174–178. https://doi.org/10.1126/science.1244341

Goyal, R., Gupta, A. S., Jucker, M., & England, M. H. (2021). Historical and projected changes in the Southern Hemisphere surface westerlies. *Geophysical Research Letters*, *48*(4), e2020GL090849. https://doi.org/10.1029/2020gl090849

Haigh, M., & Holland, P. R. (2024). Data for Decadal variability of ice-shelf melt in the Amundsen Sea driven by freshwater fluxes [Dataset]. *Zenodo*. https://doi.org/10.5281/ZENODO.10391364

Haigh, M., Holland, P. R., & Jenkins, A. (2023). The influence of bathymetry over heat transport onto the Amundsen Sea continental shelf. *Journal of Geophysical Research: Oceans*, *128*(5), e2022JC019460. https://doi.org/10.1029/2022jc019460

Henley, B. J., Gergis, J., Karoly, D. J., Power, S., Kennedy, J., & Folland, C. K. (2015). A tripole index for the interdecadal Pacific oscillation. *Climate Dynamics*, *45*(11–12), 3077–3090. https://doi.org/10.1007/s00382-015-2525-1

Hersbach, H., Bell, B., Berrisford, P., Hirahara, S., Horányi, A., Muñoz-Sabater, J., et al. (2020). The ERA5 global reanalysis. *Quarterly Journal of the Royal Meteorological Society*, *146*(730), 1999–2049. https://doi.org/10.1002/qj.3803

Heywood, K., Biddle, L., Boehme, L., Dutrieux, P., Fedak, M., Jenkins, A., et al. (2016). Between the devil and the deep blue sea: The role of the Amundsen Sea continental shelf in exchanges between ocean and ice shelves. *Oceanography*, *29*(4), 118–129. https://doi.org/10.5670/oceanog.2016.104

Holland, P. R., Bracegirdle, T. J., Dutrieux, P., Jenkins, A., & Steig, E. J. (2019). West Antarctic ice loss influenced by internal climate variability and anthropogenic forcing. *Nature Geoscience*, *12*(9), 718–724. https://doi.org/10.1038/s41561-019-0420-9

Holland, P. R., O'Connor, G. K., Bracegirdle, T. J., Dutrieux, P., Naughten, K. A., Steig, E. J., et al. (2022). Anthropogenic and internal drivers of wind changes over the Amundsen Sea, West Antarctica, during the 20th and 21st centuries. *The Cryosphere*, *16*(12), 5085–5105. https://doi.org/10.5194/tc-16-5085-2022

Jacobs, S. S. (1991). On the nature and significance of the Antarctic Slope Front. *Marine Chemistry*, *35*(1–4), 9–24. https://doi.org/10.1016/s0304-4203(09)90005-6

Jacobs, S. S., Hellmer, H. H., & Jenkins, A. (1996). Antarctic ice sheet melting in the Southeast Pacific. *Geophysical Research Letters*, *23*(9), 957–960. https://doi.org/10.1029/96gl00723

Jenkins, A., Dutrieux, P., Jacobs, S., Steig, E., Gudmundsson, H., Smith, J., & Heywood, K. (2016). Decadal Ocean forcing and Antarctic ice sheet response: Lessons from the Amundsen Sea. *Oceanography*, *29*(4), 106–117. https://doi.org/10.5670/oceanog.2016.103

Jenkins, A., Shoosmith, D., Dutrieux, P., Jacobs, S., Kim, T. W., Lee, S. H., et al. (2018). West Antarctic ice sheet retreat in the Amundsen Sea driven by decadal oceanic variability. *Nature Geoscience*, *11*(10), 733–738. https://doi.org/10.1038/s41561-018-0207-4

Joughin, I., Smith, B. E., & Medley, B. (2014). Marine ice sheet collapse potentially under way for the Thwaites Glacier Basin, West Antarctica. *Science*, *344*(6185), 735–738. https://doi.org/10.1126/science.1249055

Jourdain, N. C., Mathiot, P., Burgard, C., Caillet, J., & Kittel, C. (2022). Ice shelf basal melt rates in the Amundsen Sea at the end of the 21st century. *Geophysical Research Letters*, *49*(22), e2022GL100629. https://doi.org/10.1029/2022gl100629

Kimura, S., Jenkins, A., Regan, H., Holland, P. R., Assmann, K. M., Whitt, D. B., et al. (2017). Oceanographic controls on the variability of ice-shelf basal melting and circulation of glacial meltwater in the Amundsen Sea Embayment, Antarctica. *Journal of Geophysical Research: Oceans*, *122*(12), 10131–10155. https://doi.org/10.1002/2017jc012926

Lachlan-Cope, T., & Connolley, W. (2006). Teleconnections between the tropical Pacific and the Amundsen-Bellinghausens Sea: Role of the El Niño/Southern Oscillation. *Journal of Geophysical Research*, *111*(D23), D23101. https://doi.org/10.1029/2005jd006386

Li, X., Cai, W., Meehl, G. A., Chen, D., Yuan, X., Raphael, M., et al. (2021). Tropical teleconnection impacts on Antarctic climate changes. *Nature Reviews Earth & Environment*, *2*(10), 680–698. https://doi.org/10.1038/s43017-021-00204-5

Moorman, R., Morrison, A. K., & McC. Hogg, A. (2020). Thermal responses to Antarctic ice shelf melt in an eddy-rich global ocean–sea ice model. *Journal of Climate*, *33*(15), 6599–6620. https://doi.org/10.1175/jcli-d-19-0846.1

Naughten, K. A., Holland, P. R., & De Rydt, J. (2023). Unavoidable future increase in West Antarctic ice-shelf melting over the twenty-first century. *Nature Climate Change*, *13*(11), 1222–1228. https://doi.org/10.1038/s41558-023-01818-x

Naughten, K. A., Holland, P. R., Dutrieux, P., Kimura, S., Bett, D. T., & Jenkins, A. (2022). Simulated twentieth-century ocean warming in the Amundsen Sea, West Antarctica. *Geophysical Research Letters*, *49*(5), e2021GL094566. https://doi.org/10.1029/2021gl094566

Newman, M., Alexander, M. A., Ault, T. R., Cobb, K. M., Deser, C., Di Lorenzo, E., et al. (2016). The Pacific decadal oscillation, revisited. *Journal of Climate*, *29*(12), 4399–4427. https://doi.org/10.1175/jcli-d-15-0508.1

Rignot, E., Mouginot, J., Morlighem, M., Seroussi, H., & Scheuchl, B. (2014). Widespread, rapid grounding line retreat of Pine Island, Thwaites, Smith, and Kohler glaciers, West Antarctica, from 1992 to 2011. *Geophysical Research Letters*, *41*(10), 3502–3509. https://doi.org/10.1002/2014gl060140

Shepherd, A., Ivins, E., Rignot, E., Smith, B., van den Broeke, M., & Velicogna, I. (2018). Mass balance of the Antarctic ice Sheet from 1992 to 2017. *Nature*, *558*(7709), 219–222. https://doi.org/10.1038/s41586-018-0179-y

Si, Y., Stewart, A. L., & Eisenman, I. (2023). Heat transport across the Antarctic Slope Front controlled by cross-slope salinity gradients. *Science Advances*, *9*(18), eadd7049. https://doi.org/10.1126/sciadv.add7049

Silvano, A., Holland, P. R., Naughten, K. A., Dragomir, O., Dutrieux, P., Jenkins, A., et al. (2022). Baroclinic ocean response to climate forcing regulates decadal variability of ice-shelf melting in the Amundsen Sea. *Geophysical Research Letters*, *49*(24), e2022GL100646. https://doi.org/10.1029/2022gl100646

Spence, P., Griffies, S. M., England, M. H., Hogg, A. M., Saenko, O. A., & Jourdain, N. C. (2014). Rapid subsurface warming and circulation changes of Antarctic coastal waters by poleward shifting winds. *Geophysical Research Letters*, *41*(13), 4601–4610. https://doi.org/10.1002/2014gl060613

Steig, E., Ding, Q., Battisti, D., & Jenkins, A. (2012). Tropical forcing of circumpolar deep water inflow and outlet glacier thinning in the Amundsen Sea Embayment, West Antarctica. *Annals of Glaciology*, *53*(60), 19–28. https://doi.org/10.3189/2012aog60a110

Stewart, A. L., Klocker, A., & Menemenlis, D. (2019). Acceleration and overturning of the Antarctic Slope Current by winds, eddies, and tides. *Journal of Physical Oceanography*, *49*(8), 2043–2074. https://doi.org/10.1175/jpo-d-18-0221.1

Thoma, M., Jenkins, A., Holland, D., & Jacobs, S. (2008). Modelling circumpolar deep water intrusions on the Amundsen Sea continental shelf, Antarctica. *Geophysical Research Letters*, *35*(18), L18602. https://doi.org/10.1029/2008gl034939

Wåhlin, A. K., Kalén, O., Arneborg, L., Björk, G., Carvajal, G. K., Ha, H. K., et al. (2013). Variability of warm deep water inflow in a submarine trough on the Amundsen Sea shelf. *Journal of Physical Oceanography*, *43*(10), 2054–2070. https://doi.org/10.1175/jpo-d-12-0157.1

Walker, D. P., Brandon, M. A., Jenkins, A., Allen, J. T., Dowdeswell, J. A., & Evans, J. (2007). Oceanic heat transport onto the Amundsen Sea shelf through a submarine glacial trough. *Geophysical Research Letters*, *34*(2), L02602. https://doi.org/10.1029/2006gl028154

Walker, D. P., Jenkins, A., Assmann, K. M., Shoosmith, D. R., & Brandon, M. A. (2013). Oceanographic observations at the shelf break of the Amundsen Sea, Antarctica. *Journal of Geophysical Research: Oceans*, *118*(6), 2906–2918. https://doi.org/10.1002/jgrc.20212

Webber, B. G. M., Heywood, K. J., Stevens, D. P., & Assmann, K. M. (2019). The impact of overturning and horizontal circulation in Pine Island trough on ice shelf melt in the eastern Amundsen Sea. *Journal of Physical Oceanography*, *49*(1), 63–83. https://doi.org/10.1175/jpo-d-17-0213.1